MedCrave
Step into the World of Research

International Journal of Hydrology

Research Article

Open Access

CrossMark

A timely efficient and robust multi-source and multi-temporal routine for determination of surface water area in large water reservoirs

Abstract

The Brazilian electrical system has gone through conflicts resulting from recent water crisis. Timely indicators are crucial for properly acting in order to mitigate upcoming problems. In this work we evaluate the potential of Reservoir Water Level (RWL) and Surface Water Area (SWA) indices for estimating physical parameters in the management of water resources. We tested Landsat 8 (L8) and Sentinel-2 (S2) optical image time series, Sentinel-1 (S1) radar, spectral indices and validation with Jason-3 (J3) altimetry. The methodology was developed in the Google Earth Engine (GEE) operational routine, which streamlined the SWA mapping. The best results were between S2 and NDWI and threshold 0, with $R^2 = 0.88$ and RMSE of 11.59 km². As main limitations, we highlight the cloud cover for the optical images, which can decrease the temporal sampling, as well as the SAR backscatter response in the presence of bare soil and aquatic vegetation. We could attest that periodic remote sensing data are particularly useful for timely updating spatial variations of RWL and SWA in reservoirs.

Keywords: water resources, spectral indexes, google earth engine, sentinel-1, sentinel-2, landsat 8, Jason-3

Volume 6 Issue 5 - 2022

Douglas Stefanello Facco,[1] Laurindo Antonio Guasselli,[1] Daniel Capella Zanotta,[1] Luis Fernando Chimelo Ruiz[2]

[1]Research Center on Remote Sensing and Meteorology, Federal University of Rio Grande do Sul, Brazil

[2]Research and development (R&D) at Santos Lab Digital, Brazil

Correspondence: Douglas Stefanello Facco, Research Center on Remote Sensing and Meteorology, Federal University of Rio Grande do Sul, Porto Alegre, Brazil, Tel 55 55 9 96236952, Email douglas.s.facco@gmail.com

Received: September 30, 2022 | **Published:** October 12, 2022

Introduction

The Brazil has experienced water crises that have affected human supply, agriculture, navigability and energy generation.[1] According to[2] conflicts involving the Brazilian Electric System are caused by recent water crisis involving their companies and their management sector. As popularly known, most of it is caused by critical low dam reservoirs levels. Sedimentation is another important reason that affects the level of dam reservoirs, being the most important factor in reducing the volume and their useful life.[3] Reservoir Water Level (RWL) and Surface Water Area (SWA) are crucial physical parameters in water resource management, and stand for good indicators of climate change impacts.[4–6] Accurate and up-to-date databases on RWL and SWA and their spatial distribution are needed in surface water mapping, periodic estimates for consumption and irrigation, wetland conservation, and ecological environmental assessment.[7] Traditional approaches to monitoring RWL in reservoirs use in situ measurement. However, in large reservoirs, it is impractical to install and maintain the sufficient number of measurement stations.[8,9] It is necessary a huge amount of measuring devices to monitor every subbasin and finally compute the entire reservoir volume. Althought, water level is found to be intimately associated with superficial area for a particular reservoir and can be adequately used to estimate RWL.[10–12]

Remote sensing (RS) data is ideal for estimating SWA. Relationship between RWL and SWA in reservoirs, derived from orbital sensors, allows the estimation of these parameters based on the dynamic behavior of the covering area. Many studies have demonstrated that Optical L8 and S2 images are very useful to separate the water sheet from other covers.[13] Although, there are several methods for water volume and level estimation, they lack generalization. One reason is that there are widespread differences in the parameters of many remote sensing sensors, and classification rules are often defined for remote sensing images from several sensors.[14]

Literature has demonstrated that differences in reflectivity for water and non-water bodies can be adequately extracted from spectral indices.[15] Spectral water indices are more accurate compared to other methods such as classification techniques, or linear unmixing.[7,16,17] Among the spectral indices of water most used in the literature, in[18] the authors developed the Normalized Difference Water Index (NDWI) using green and near-infrared (NIR) spectral ranges to maximize water characteristics.[18] replaced NIR with shortwave infrared (SWIR) and derived the modified NDWI (MNDWI).

Radar images are used to separate water sheets from other covers, with the advantage that clouds and fog are not a concern.[20] Radar backscatter is sensitive to the moisture content and harshness of the landscape. The Sentinel-1 sensor's C-band penetrates clouds and thick canopies.[21] Satellite altimetry (RA), originally used for ocean surface topography, has been tested for rivers, lakes, and reservoirs with great results.[22] In the case of small reservoirs, the precision of water level time series derived from satellite altimetry is mainly ruled by the seasonal variability of the water storage.[23]

The cloud-based platform Google Earth Engine (GEE) is very convenient in large-scale analysis to understand long-term[24] changes in reservoirs.[25] There are many advantages for using radar data over optical satellite data. The wavelength of the radar signal together with the active satellite sensor allows data acquisition at any time of the day and regardless of weather conditions.[26] Bodies of water are seen as dark regions in the image, due to the reduced back scattering of the radio signal transmitted from a smooth surface. The roughness of the water is what defines its value and not its color properties as we are used to with optical images.[26]

In this work, we aim to employ a large-scale multi-source and multi-temporal database to estimate RWL and SWA in reservoirs using consolidated estimation metrics based on invariant indices and remote sensing data. For optical imaging, the water spectral index method is a multiband extraction method commonly used in remote sensing to select significance thresholds between a body of water and non-water. For radar images, backscatter data is used, appropriate thresholds in decibels (dB) are selected to measure wave scattering.

Based on L8 and S2 optical images of 30 meters and 10 meters of spatial resolution respectively, S1 radar images of 10 meters and J3 altimetry data with 3.3 cm accuracy used for validation, satellite measurements (or orbital data) are used to update the spatial and temporal variations of SWA in reservoirs. Studies have already tested the accuracy of the estimates of these sensors separately, but none has verified the accuracy of both for a reservoir, indicating the best parameters and thresholds, operating within a dynamic, accessible, fast and free cloud platform.

Materials and methods

We selected as a study area the reservoir of the Itaipu hydroelectric plant, located in South America on the Brazil-Paraguay border (Figure 1). The Itaipu Reservoir, one of the largest producers of hydroelectric power in the world, is located in the western region of the State of Paraná, in southern Brazil. The reservoir is 170 km² long, has an average width of 7 km, an average depth of 22 m, 170 m close to the dam, a minimum water level of 197 m and a maximum of 220 m. The Itaipu dam is the most down-stream in the Paraná Basin, and receives a positive contribution from all Paraná Basin reservoirs. Regardless of change in the country's energy storage, the flooded area of the reservoirs around Itaipu, does not vary substantially.[26]

Figure 1 (a) Location of the Itaipu reservoir (red square) in relation to South America; (b) Regional location of the Itaipu reservoir on the Brazil-Paraguay border; (c) Expanded map of the extension of the Itaipu reservoir.

The climate of the western region of Paraná State is classified as humid subtropical (Cfa, according to the Köppen classification). The average monthly temperature is above 22°C in the summer period. The average annual precipitation varies from 1600 to 1700 mm in the studied region. Agriculture is the main land use in the basin area. The predominant soil type is the Latosol, which corresponds to soils in advanced stages of weathering, typical of both equatorial and tropical regions, also occurring in sub-tropical zones. Latosols are mainly distributed over large and old erosion surfaces or river terraces, usually in flat and undulating relief.[28]

Methodological flowchart

The flowchart shown in Figure 2 provides the general structure of the pipeline methodology for determining the surface water area in large reservoirs. Methodology steps will be detailed in what follows.

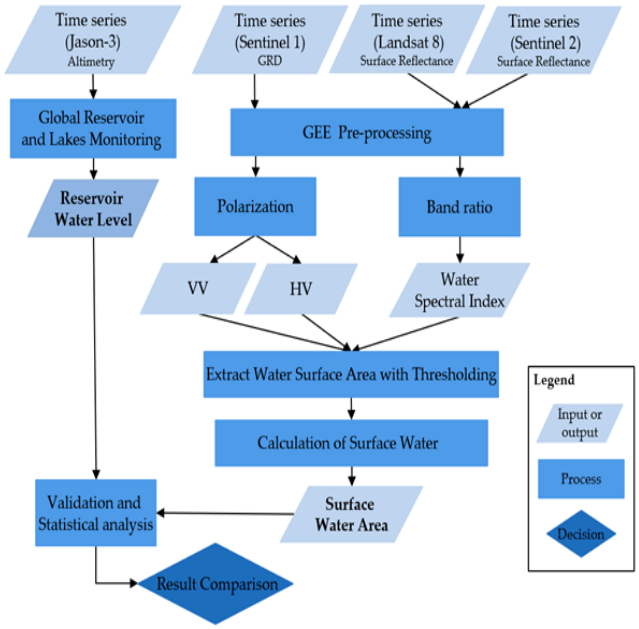

Figure 2 Summary flowchart of the methodology.

Data set: time series of satellite imagery and altimetry

We used data from synthetic aperture radar S1 and multispectral L8 and S2 images, processed in the GEE platform. All the data was validated using J3 altimeter. The analysis period was between 2019 and 2021, due to the availability of S2. Images have a maximum delay of 5 days with J3. The products used are described below.

a) S1: C-band data from Sentinel-1 in Interferometric Wide Swath (IW) mode was designed to acquire images of Earth surfaces. In IW mode it has dual polarization with vertical transmission and vertical reception (VV) and vertical transmission and horizontal reception (VH) and spatial resolution of 10-meter. We used the Level 1 Ground Range Detected (GRD) product pre-processed in the GEE to derive the backscatter co-efficient at each pixel. The VV and VH polarized data were selected to map the water surface. To cover the reservoir, it was necessary to mosaic two SAR images for each date, totaling 66 dates;

b) L8: The Landsat 8 Surface Reflectance Tier 1 multispectral images available on the GEE are derived from the Landsat 8 OLI / TIRS sensors. The images were orthorectified and atmospherically corrected to obtain surface reflectance. The bands used were 3 (green), 4 (red), 5 (near infrared) and 6 (medium infrared) with a spatial resolution of 30 meters. Two Lansdat-8 images were merged to cover the reservoir on each date, totaling 16 dates;

c) S2: S2 multispectral images with level 2A processing are available in the GEE, orthorectified and atmospherically corrected for surface reflectance values. Bands 3 (green), 4 (red) and 8 (near infrared) with a spatial resolution of 10-meter and band 11 (short wave infrared) of 20-meter were used. To cover the reservoir, it was necessary to merge 3 Sentinel-2 images for each analyzed date, totaling 33 dates;

d) Jason-3: RWL data acquired every 10 days from the US Department of Agri-culture, Global Reservoirs and Lakes Monitor website (USDA G-REALM; https://ipad.fas.usda.gov/cropexplorer/global_reservoir) was used for validation, due to its high accuracy and consistency with 3.3 cm in reservoirs with a width greater than 100 m.[29,22,30]

Generation of SWA time series

GEE combines a multi-petabyte catalog of satellite imagery and geospatial datasets with planetary-scale analysis capabilities.[31,32] Scientists, researchers, and developers use Earth Engine to detect changes, map trends, and quantify differences on the Earth's surface. The GEE hosts complete and up-to-date S1, S2, and L8 data files. We produced temporally distributed water masks and calculate the maximum SWA extent included for each date, with selection of suitable thresholds. As mentioned before, water bodies are determined by texture levels in radar images. For S1, we used thresholds between -24 and -18 decibels (dB) in the VH band and between -15 and -5 dB in the VV band.[33] For S2 and L8, the water spectral index method is a commonly used multi-band extraction method, which is combined with other remote sensing indices to select the threshold of significant difference between a water body and a non-water body. We used the spectral index NDWI[18] Eq (1) and MNDWI[19] Eq (2), widely used and robust in water extraction, and applied suitable thresholds for water and non-water pixels 0.0, 0.1, and 0.2.

$$NDWI = (Green-NIR)/(Green+NIR) \quad (1)$$

$$MNDWI = (Green-SWIR)/(Green+SWIR) \quad (2)$$

Where: NDWI is the Normalized Difference Water Index; MNDWI is Modified Nor-malized Difference Water Index; Green is the reflected green visible light; NIR is the reflected near-infrared energy; SWIR is the reflected short-wave infrared energy.

Accuracy assessment

For each image of sensors S1, S2 and L8, the SWA was calculated for the thresholds described in section 2.3. Validation was performed using data from J3 altimetry water levels. J3 data is not as frequent as S1, S2, and L8 imagery, but some dates with occurrence of simultaneously acquisition were used for assessing purposes. In order to evaluate correlation, the coefficient of determination (R^2) and the root mean square error (RMSE) were calculated to verify the imaging sensor with the highest relation-ship with J3 for greater reliability in the SWA calculation.

Results and discussions

SWA and RWL relationship and better thresholds

Based on R^2 and RMSE (Table 1), the linear model that described the best relationship between SWA and RWL was S2 and NDWI and threshold 0, with R reaching 0.94, $R^2 = 0.88$, and RMSE =11.59 km². In general, multispectral sensors exhibited better results with L8 and NDWI and threshold 0, with R reaching 0.91, R2 = 0.83, and RMSE less than 15 km². S1 was less satisfactory in the HV band ($R^2 = 0.45$ for thresholds between -23 and -24 dB and the VV band (R^2 equals 0.61 for the -14 dB threshold). Areas near the reservoir edge were sources of S1 error, mislabeling water pixels to exposed soil and wet areas with aquatic vegetation (Figure 3), especially when the water level was lower, causing SWA overestimation.

Table 1 Relationship between SWA and RWL in the reservoir

Satellite	Parameters	Thresholds	R	R^2	RMSE Km²
Sentinel-1	HV	-24	0.67	0.45	
S1		-23	0.67	0.45	13.59
		-22	0.63	0.4	
	VV	-15	0.73	0.53	
		-14	0.78	0.61	14.37
		-13	0.75	0.57	
Landsat 8	MNDWI	0	0.91	0.83	14.46
L8		0.1	0.91	0.82	
		0.2	0.9	0.81	
	NDWI	0	0.9	0.81	
		0.1	0.91	0.82	16.85
		0.2	0.87	0.75	
Sentinel-2	MNDWI	0	0.93	0.87	11.98
S2		0.1	0.93	0.86	
		0.2	0.93	0.86	
	NDWI	0	0.94	0.88	11.59
		0.1	0.93	0.86	
		0.2	0.9	0.81	

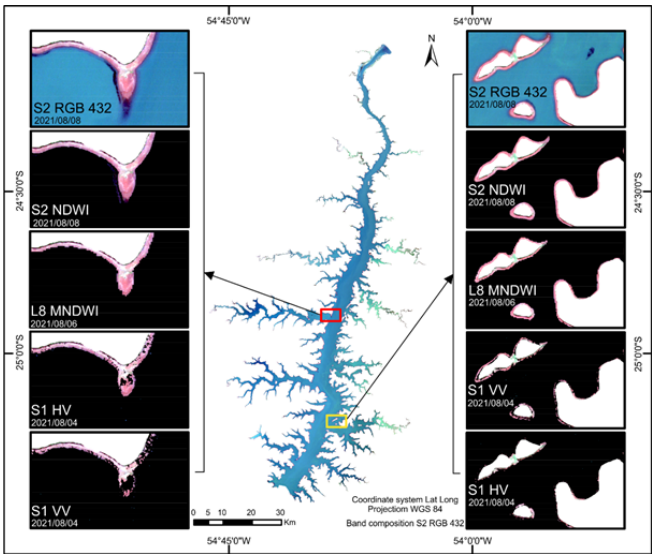

Figure 3 In the center of the Image: Spatial distribution of the water surface of the Itaipu reservoir on the date 08/08/2021 in true RGB432 composition by the S2 sensor SWA and RWL time series. In the column on the left we have a comparison between the sensors with their best parameters for the region the (red rectangle). in the column on the right we have a comparison between the sensors with their best parameters for the region (yellow rectangle).

Water spectral indices for determining SWA are important for establishing the optimal threshold for separating water and non-water pixels.[34] The optimal index depends on the environmental characteristics of the study area, including topography and shadows.[35] The factors that affect the quality of the water mask are different in optical and radar observations. In S1, water detection occurs in low-backscatter areas.[36] When the water body is near wetlands, the SAR response affects low-signal zones on water surfaces.[36] Our results agree with[37] that VV polarization is better for differentiating water and non-water areas compared to VH. Among multispectral sensors, our results agree with,[38,39] which state that S2 is better than L8 considering its spatial and spectral ability to identify water pixels and other coverages. In[40,9] the authors used Landsat 8 water spectral indices to analyze the spatio temporal dynamics of the reservoir.

Both SWA and RWL time series were derived from S2 and J3, which obtained the best discriminating features. Figure 4 contains 33 points, representing the time lapse between 2019 and 2022. The SWA ranged between 1140.2 Km² and 1271.51 km², and the RWL ranged between 215.69 m and 220 m. Figure 4 shows the S2 time series of SWA and RWL, while Figure 5 shows the scatterplot of the S2 and J3 data. The works of[41,42] found that satellite imagery allows the analysis of spatiotemporal variability in res-ervoirs without the requirement of in situ data. A major advance in studying reservoirs with no ground-based observations. J3 data have an error of fewer than 0.30 m and are satisfactory for water height in reservoirs wider than 100 meters.[26,20,28] In this study, the maximum time lag between the orbital image acquisition and the J3 passage was 5 days. Longer delay may lead to an increased SWA detection error. Using J3 for validation was appropriate due to its high accuracy[22,30] while using GEE allowed automating the methodology and process large datasets (Big Earth Data).[43]

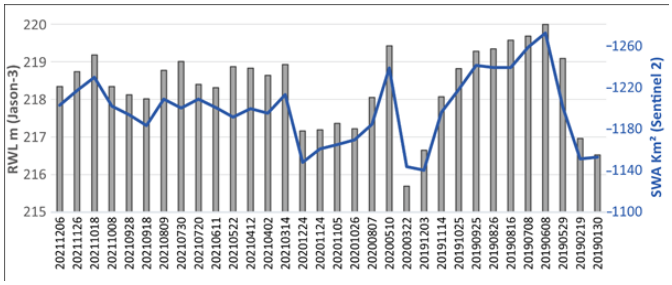

Figure 4 SWA and RWL time series. The gray columns represent the reservoir level in m by the J3 sensor, and the blue line represents the surface area data in Km² by the Sentinel 2.

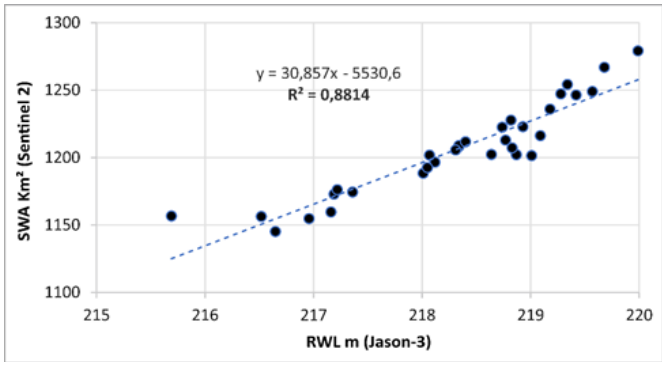

Figure 5 Scatterplot showing the relationship between SWA (Sentinel 2) and RWL (Janson-3) data.

Conclusion

This paper presented an approach to estimating the time series of SWA and RWL variations in reservoirs by combining orbital imagery processed in GEE and J3 altimetry. GEE expedited the mapping of SWA and allowed significantly reduced time and costs in reservoir monitoring. Assessing showed considerable agreement between estimated and observed measures, while SWA and RWL time series from S2 and J3 obtained the best settings. The indirect estimation of important reservoir parameters is able to provide a rapid and reliable water condition. As main limitations, we highlight the cloud cover for the optical images, which can decrease temporal sampling, as well the SAR backscatter response in the presence of bare soil and aquatic vegetation.

Acknowledgments

None.

Conflicts of interest

The author declares there is no confclit of interest.

References

1. Mining 2021. *Water crisis threatens iron transport on key Brazil river*. 2021.
2. Galvão J, Bermann C. Crise hídrica e energia: conflitos no uso múltiplo das águas. *Estudos avançados.* 2015;29:43–68.
3. Mahmoodieh N, Ghomeshi M. Investigation the effect of concentration and radius of bend curvature on turbidity current body thickness in 90 degree bend. *Irrigation Sciences and Engineering.* 2019.
4. Pekel JF, Cottam A, Gorelick N, et al. High-resolution mapping of global surface water and its long-term changes. *Nature.* 2016;540:418–22.
5. Sun S, Wang Y, Liu J, et al. Sustainability assessment of regional water resources under the DPSIR framework. *Journal of Hydrology.* 2016;532:140–148.
6. Liu KT, Tseng KH, Shum CK, et al. Assessment of the impact of reservoirs in the upper Mekong River using satellite radar altimetry and remote sensing imageries. *Remote Sensing* 2016;8:367.
7. Acharya TD, Subedi A, Lee DH. Evaluation of Water Indices for Surface Water Extraction in a Landsat 8 Scene of Nepal. *Sensors.* 2018;18:2580.
8. Beskow S, Timm LC, Tavares VEQ. Potential of the LASH model for water resources management in data-scarce basins: a case study of the Fragata River basin, southern Brazil. *Hydrological Sciences Journal* 2016;61:2567–2578.
9. Facco DS, Guasselli LA, Ruiz LFC, et al. Spectral Reflectance in the Spatial-temporal Dynamic of Turbidity, Itaipu Reservoir, Brazil. *Anuário do Instituto de Geociências* 2021;44.
10. Li J, Wang S. An automatic method for mapping inland surface waterbodies with Radarsat-2 imagery. *International Journal of Remote Sensing* 2015;36:1367–1384.
11. Pipitone C, Maltese A, Dardanelli G, et al. Monitoring Water Surface and Level of a Reservoir Using Different Remote Sensing Approaches and Comparison with Dam Displacements Evaluated *via* GNSS. *Remote Sensing.* 2018;10:71.
12. Yuan C, Gong P, Liu C, et al. Water-volume variations of Lake Hulun estimated from serial Jason altimeters and Landsat TM/ETM+ images from 2002 to 2017. *International Journal of Remote Sensing.* 2018;40:670–692.
13. Cavallo C, Papa MN, Gargiulo M, et al. Continuous Monitoring of the Flooding Dynamics in the Albufera Wetland (Spain) by Landsat-8 and Sentinel-2 Datasets. *Remote Sensing.* 2021;13:3525.
14. Li J, Ma R, Cao Z, et al. Satellite Detection of Surface Water Extent: A Review of Methodology. *Water.* 2022;14:1148.
15. Santoro M, Wegmüller U, Lamarche C, et al. Strengths and weaknesses of multi-year Envisat ASAR backscatter measurements to map permanent open water bodies at global scale. *Remote Sensing of Environment.* 2015;171:185–201.
16. Şerban C, Maftei C, Dobrică G. Surface Water Change Detection via Water Indices and Predictive Modeling Using Remote Sensing Imagery: A Case Study of Nuntasi-Tuzla Lake, Romania. *Water.* 2022;14:556.
17. Yang X, Chu Q, Wang L, et al. Water Body Super-Resolution Mapping Based on Multiple Endmember Spectral Mixture Analysis and Multiscale Spatio-Temporal Dependence. *Remote Sens.* 2022;14:2050.
18. McFeeters SK. The use of the Normalized Difference Water Index (NDWI) in the delineation of open water features. *International journal of remote sensing.* 1996;17(7):1425–1432.

19. Xu H. Modification of normalised difference water index (NDWI) to enhance open water features in remotely sensed imagery. *International journal of remote sensing* 2006;27(14):3025–3033.

20. Zhou S, Kan P, Silbernagel J, Jin J. Application of Image Segmentation in Surface Water Extraction of Freshwater Lakes using Radar Data. *ISPRS International Journal of Geo-Information* 2020;9:424.

21. Bioresita F, Puissant A, Stumpf A, et al. A Method for Automatic and Rapid Mapping of Water Surfaces from Sentinel-1 Imagery. *Remote Sensing*. 2018;10:217.

22. Biancamaria S, Schaedele T, Blumstein D, et al. Validation of Jason-3 tracking modes over French rivers. *Remote Sensing of Environment.* 2018;209:77–89.

23. Neto AR, Behnia S, Tourian MJ, et al. Satellite altimetry over small reservoirs in the Brazilian semiarid region. *Revista Brasileira de Recursos Hídricos* 2021;26.

24. Amani M, Ghorbanian A, Ahmadi SA, et al. Google earth engine cloud computing platform for remote sensing big data applications: A comprehensive review. *IEEE Journal of Selected Topics in Applied Earth Observations and Remote Sensing.* 2020;13:5326–5350.

25. Deng Y, Jiang W, Tang Z, et al. Long-Term Changes of Open-Surface Water Bodies in the Yangtze River Basin Based on the Google Earth Engine Cloud Platform. *Remote Sensing.* 2019;11:2213.

26. Čotar K, Oštir K, Kokalj Ž. Radar Satellite Imagery and Automatic Detection of Water Bodies. *Geode Glass* 2016;50:5–15.

27. Hunt JD, Falchetta G, Zakeri B, et al. Hydropower impact on the river flow of a humid regional climate. *Climatic Change.* 2020;163:379–393.

28. Rocha ASD, Bade MR. *Geografia da bacia hidrográfica do Paraná 3: fragilidades e potencialidades socioambientais,* 3rd edn. Publisher: In House. Jundiaí, São Paulo, Brazil, 2018;314.

29. Le Gac S, Boy F, Blumstein D. *Update and validation of Jason-3 onboard DEM: Enhanced acquisitions over inland water targets, Presentation at OSTST Meeting*. Miami, USA, 2017.

30. Le Gac S, Boy F, Blumstein D, et al. Benefits of the Open-Loop Tracking Command (OLTC): Extending conventional nadir altimetry to inland waters monitoring. *Advances in Space Research.* 2021;68:843–852.

31. Gorelick N, Hancher M, Dixon M, et al. Google Earth Engine: Planetary-scale geospatial analysis for everyone. *Remote sensing of Environment* 2017;202:18–27.

32. Abujayyab SKM, Almotairi KH, Alswaitti M, et al. Effects of Meteorological Parameters on Surface Water Loss in Burdur Lake, Turkey over 34 Years Landsat Google Earth Engine Time-Series. *Land.* 2021;10:1301.

33. Manjusree P, Prasanna Kumar L, Bhatt CM, et al. Optimization of threshold ranges for rapid flood inundation mapping by evaluating backscatter profiles of high incidence angle SAR images. *International Journal of Disaster Risk Science.* 2012;3:113–122.

34. Özelkan E. Water body detection analysis using NDWI indices derived from landsat-8 OLI. *Polish Journal of Environmental Studies.* 2020;29:1759–1769.

35. Zhai K, Wu X, Qin Y, et al. Comparison of surface water extraction performances of different classic water indices using OLI and TM imageries in different situations. *Geo-spatial Information Science.* 2015;18(1):32–42.

36. Peña-Luque S, Ferrant S, Cordeiro MCR, et al. Sentinel-1&2 Multitemporal Water Surface Detection Accuracies, Evaluated at Regional and Reservoirs Level. *Remote Sensing.* 2021;13:3279.

37. Pôssa ÉM, Maillard P, Gomes MF, et al. *On water surface delineation in rivers using Landsat-8, Sentinel-1 and Sentinel-2 data*. In Proceedings of Conference Remote Sensing for Agriculture, Ecosystems, and Hydrology XX, Berlin, Germany, 10 Oct 2018.

38. Marangoz AM, Sekertekin A, Akçin H. *Analysis of land use land cover classification results derived from sentinel-2 image*. In Proceedings of the 17th International Multidisciplinary Scientific GeoConference Surveying Geology and Mining Ecology Management, SGEM 2017, Albena and Varna, Bulgaria, 2017. p. 25–32.

39. Ahady AB, Kaplan G. Classification comparison of Landsat-8 and Sentinel-2 data in Google Earth Engine, study case of the city of Kabul. *International Journal of Engineering and Geosciences.* 2022;7:24–31.

40. Facco DS, Guasselli LA, Ruiz LFC, et al. Comparison of PBIA and GEOBIA classification methods in classifying turbidity in reservoirs. *Geocarto International.* 2021;37(16):1–22.

41. Biancamaria S, Lettenmaier DP, Pavelsky TM. The SWOT mission and its capabilities for land hydrology. *Remote sensing and water resources.* 2016;117–147.

42. Bonnema M, F Hossain. Inferring reservoir operating patterns across the Mekong Basin using only space observations. *Water Resources Research.* 2017;53:3791–3810.

43. Sun Z, Luo J, Yang J, et al. Nation-Scale Mapping of Coastal Aquaculture Ponds with Sentinel-1 SAR Data Using Google Earth Engine. *Remote Sens.* 2020;12:3086.